International Journal of Basic and Applied Sciences, 14 (2) (2025) 132-144

International Journal of Basic and Applied Sciences

Website: www.sciencepubco.com/index.php/IJBAS
https://doi.org/10.14419/7q1jcv93
Research paper



Design and Development of Meta-Heuristic Transfer Learning Techniques for Ovarian Cancer Detection

V. Sathiyavani [1] *, Dr. Vinothkumar Arumugam [2], Dr. M Anand [2]

[1] Research Scholar, Dept. of ECE, Dr. M.G.R Educational & Research Institute, India
[2] Professor, Dept. of ECE, Dr. M.G.R Educational & Research Institute, India.
**Corresponding author E-mail: sathiyavani25061983@gmail.com*

Received: May 6, 2025, Accepted: May 22, 2025, Published: June 10, 2025

Abstract

Cancer continues to claim a significant number of lives globally, with ovarian cancer being particularly deadly owing to its late-stage diagnosis and limited availability of effective treatments. Current diagnostic methods often rely on traditional imaging and histopathological analysis, which face challenges such as limited accuracy, high false-positive rates, and dependency on expert interpretation. Though artificial intelligence techniques have addressed this bottleneck, achieving higher performance with low computational overhead remains a significant challenge in current research. To rectify these drawbacks, this research recommends a hybrid approach leveraging transfer learning models such as Inception V3 and Improved Black Widow Optimized dense classification layers to enhance diagnosis performance. The model was trained and validated using the UBC-OCEAN dataset, which consists of 5,634 standardized samples classified into three primary ovarian cancer subtypes: high-grade serous carcinoma (3,412 samples), endometrioid carcinoma (1,732 samples), and clear cell carcinoma (490 samples), alongside rare outlier cases for anomaly detection. The comprehensive outcomes portray the recommended approach attained the classification accuracy of 98.7%, with a precision of 98.7%, recall of 98.7%, and an F1-score of 98.7%, demonstrating enhanced performance compared to conventional Deep Learning (DL) approaches. The integration of metaheuristic optimization further refined the classification process, enhancing model performances and robustness. The results emphasize the model's efficacy as a reliable tool for early detection and subtype identification, and deployment in clinical workflows, offering scalability and ease of integration into existing diagnostic pipelines, ultimately contributing to improved patient diagnosis outcomes.

Keywords: *Black Widow Optimization; Cancer Detection; Classification; Inception V3; Metaheuristic; Ovarian Cancer; Transfer Learning; UBC-OCEAN Dataset.*

1. Introduction

Ovarian cancer has emerged as deadliest cancers affecting women worldwide, posing a significant health threat. With an alarming rise in incidence rates, ovarian cancer is now the fifth leading cause of cancer-related deaths among women, especially in developed countries [1-3]. Globally, it is estimated that over 300,000 women are diagnosed with ovarian cancer each year, and the numbers continue to rise. The situation is particularly concerning in countries like India, where late-stage diagnoses are common due to lack of awareness, leading to high mortality rates. In fact, ovarian cancer is often detected at advanced stages, making it harder to treat effectively. The prognosis for ovarian cancer patients is poor, with a 5-year survival rate of around 45%, largely due to the lack of early detection methods [4].

Early and accurate detection of ovarian cancer remains the most effective strategy for improving survival rates. However, current diagnostic methods such as ultrasound, CT scans, and biopsy often lack the sensitivity and specificity required for early detection, especially in high-risk groups [5], [6]. Moreover, these methods can be time-consuming, expensive, and prone to human error, leading to delays in treatment and suboptimal outcomes for patients. Given these challenges, there is an urgent need for advanced computational methods to aid in the early diagnosis and classification of ovarian cancer [7].

Recent advancements in Machine Learning (ML) and DL have shown promising potential in automating the process of ovarian cancer detection. Convolutional Neural Networks (CNNs), known for their competence in independently recognizing features from images, play a crucial role in analysing medical images for cancer detection [8,9]. Transfer learning approaches, which leverage pre-trained models on large datasets to transfer knowledge to smaller datasets, have yielded excellent outcomes in medical image classification tasks. Specifically, the Inception V3 model, a Cutting edge DL approach, has been successfully applied to various cancer detection tasks, including ovarian cancer, to achieve improved accuracy and efficiency in identifying cancerous regions in medical images. However, optimizing these models for better performance remains a challenge, especially when dealing with small and imbalanced datasets [10-12].

Optimization techniques are essential in addressing these challenges by fine-tuning the parameters of the model to achieve optimal performance. The Hybrid Optimization approach, a recent metaheuristic optimization approach, has demonstrated its ability to optimize the search for ideal outcomes in multifaceted, high-dimensional spaces. Applying optimization alongside transfer learning models enhances

Copyright © V. Sathiyavani et al. This is an open access article distributed under the Creative Commons Attribution License, which permits unrestricted use, distribution, and reproduction in any medium, provided the original work is properly cited.

the performance of ovarian cancer detection systems by increasing classification accuracy, reducing false negatives, and minimizing computational complexity.

1.1. Problem formulation

Several significant challenges persist in ovarian cancer detection, particularly in achieving optimal classification performance. The primary bottleneck is the limited availability of high-quality annotated medical image datasets, which are crucial for training DL approaches. Moreover, most existing datasets are small and imbalanced, making it difficult for traditional machine learning models to generalize well. The second challenge lies in the computational complexity of deep learning models, which can result in high training times and increased risk of overfitting, particularly in the case of small datasets. These issues lead to suboptimal diagnostic accuracy and higher rates of false positives and false negatives, which can have serious issues for patient outcomes.

1.2. Motivation of the research

This research aims to address challenges in ovarian cancer detection by developing an accurate, efficient, and reliable model. Integrating transfer learning with advanced optimization techniques ensures high performance with limited data. Pre-trained models like Inception V3 reduce the reliance on large labelled datasets, while Improved optimization algorithms enhance model accuracy. The goal is to create an automated tool to assist healthcare professionals in early detection, improve survival rates, and reduce the strain on medical resources.

1.3. Research contribution

This research proposes a novel approach for ovarian cancer detection that integrates Transfer Learning with the Improved Hybrid Optimization algorithm. Specifically, the Inception V3 model is employed for feature extraction and classification, with the optimization algorithm used to optimize the model's hyperparameters for better performance. The offerings of this paper follows:

1) Transfer Learning utilizes Inception V3: The Inception V3 model, a DL approach renowned for its high performance in image classification tasks, is applied to ovarian cancer detection. Leveraging a pre-trained version of this model significantly reduces the training data requirement while achieving high classification accuracy.
2) Improved Hybrid Optimization: The improved Hybrid optimizer enhances the Inception V3 model's performance by tuning hyperparameters such as learning rate and regularization parameters. This metaheuristic optimization technique improves classification performance and minimizes overfitting.
3) Comprehensive Analysis using the UBC-OCEAN Dataset: The recommended framework is evaluated using the UBC-OCEAN dataset, comprising over 5,600 ovarian cancer image samples across three primary subtypes. The dataset supports training and testing the model, with performance metrics like precision, accuracy, F1-score and recall computed and examined against cutting edge approaches.
4) Impact of Rare and Atypical Cases: The inclusion of rare and atypical cases in the dataset enables the model to demonstrate robustness and effectively detect anomalies, addressing a critical aspect of cancer diagnosis.

1.4. Organization of the paper

The rest of the paper is ordered in the following manner: Section-2 Reviews existing research and methodologies related to ovarian cancer detection, transfer learning, and optimization techniques. Section-3 Details the dataset utilized for this study, along with the preprocessing, transfer learning, and optimization models. Section-4 Represents the implementation details, experimental setup, and outcomes of the recommended approach, including a comparative analysis with varied cutting edge approach. Section-5 wraps up the paper and discusses potential future endeavours for further improvement and research.

2. Related works

[13] developed an integrated ML diagnostic model combining feature dimensionality reduction and neural networks for ovarian cancer detection. The model utilized data from 185 cancer cases and multiple control groups. Their approach incorporated a pre-trained ResNet50 network with three edge output modules for tumor segmentation. Experimental results achieved 83.62% Dice similarity and an ROC curve area of 0.948. The study demonstrated significant improvement over traditional CA125 detection, though its reliance on a single dataset limits the model's generalizability across diverse populations.

[14] proposed a deep learning framework utilizing VGG16 and MobileNetV2 architectures with Squeeze-and-Excitation blocks for ovarian cancer subtype classification. The model was fine-tuned utilized transfer learning to classify the subtypes. Their methodology employed transfer learning from ImageNet pre-trained models to identify five major subtypes from histopathological images. The MobileNetV2 with SE blocks demonstrated enhanced performance in capturing tissue patterns, offering enhanced accuracy. Nevertheless, the model's complexity may hinder its scalability and real-time application due to high computational resource requirements.

[15] presented a dual-architecture approach combining DeepLabV3 and YOLOv8 for analyzing ovarian tumors in O-RADS US Category 4 lesions, using 1619 ultrasound images from three centers. Their methodology achieved 98.68% precision for benign masses and 96.23% for malignant masses, with consistent AUC values across training (0.96), validation (0.93), and test (0.95) sets. However, the model's performance is constrained by its reliance on a specific dataset, limiting its ability to generalize to diverse clinical settings or populations.

[16] recommends an improved DL model for ovarian cancer detection, utilizing a modified VGG-16 architecture. The model, which includes thirteen convolution layers and five maximum pooling layers, was initially trained on 500 histopathological images from four distinct ovarian cancer subtypes (Serous, Mucinous, Endometrioid, Clear Cell), resulting in a 50% accuracy rate. To enhance model performance, various image processing techniques were applied, generating an additional 24,742 images from the original dataset. After training on the expanded dataset, the model's accuracy increased to 84%. Meanwhile the need for larger dataset may increase computational costs, limiting its use in resource-limited settings.

[17] developed a fuzzy DL approach for ovarian cancer identification, utilizing a dataset of 288 H&E stained whole slides from 78 patients. Their methodology integrated ResNet-50 for feature extraction, combined with recursive feature elimination (RFE) to opt the

prominent attributes, and employed Adam optimization to enhance the model's training process. This approach achieved outstanding results, with an accuracy of 97.85%. The complexity of the fuzzy deep learning approach may lead to longer training times, which could limit its scalability in clinical settings.

[18] proposed a CNN-based framework for ovarian cancer prediction and diagnosis in pre- and post-menopausal women using histopathological images. Their approach achieved 94% accuracy with 95.09% sensitivity for cancerous cases and 92% specificity for healthy cells. The model demonstrated significant improvement over human expert examination, though the study's limitation in addressing specific menopausal status variations suggests room for refinement.

[19] introduced a novel approach that combined optical coherence tomography (OCT) with neural networks for ovarian cancer detection in transgenic mice. The methodology involved comparing three different neural network architectures: a VGG-supported feed-forward network, a 3D CNN, and a convolutional long short-term memory (LSTM) network. Among these, the convolutional LSTM network outperformed the others, achieving the optimal performance with an AUC of 0.81 ± 0.037. However, the model's accuracy was moderate compared to other advanced approaches, which may limit its competitive edge in clinical applications.

[20] developed a CNN model with a convolutional autoencoder (CNN-CAE) for ovarian tumor classification, utilizing a dataset of 1613 ultrasound images. Their approach incorporated DenseNet architectures, which helped capture intricate features in the images. The model achieved impressive results, with 97.2% accuracy and 0.9936 AUC for distinguishing normal tissues from tumors, and 90.12% accuracy with 0.9406 AUC for detecting malignant tumors. Despite these promising results, a significant drawback of the model is its high computational resource requirements, which could limit its scalability resource-constrained clinical environments.

[21] proposed a Self-Organizing Map (SOM) and Optimized Neural Networks approach for ovarian cancer detection, leveraging clinical network data. Their methodology incorporated a Feature Optimization and Identification framework, which utilized Advanced Harmony Searching Optimization (AHSO) to fine-tune the features for improved accuracy. This approach achieved impressive results, with 94% precision and 0.029% root mean square error (RMSE). Meanwhile the use of complex optimization techniques such as AHSO introduces high computational complexity, potentially limiting its efficiency and scalability for real-time clinical use.

[22] provided a comprehensive global cancer statistics report using GLOBOCAN 2018 estimates across 185 countries. The study projected 18.1 million new cancer cases and 9.6 million cancer deaths worldwide in 2018. Lung cancer ranked highest in both diagnosis (11.6% of cases) and deaths (18.4%), with female breast cancer equally common in diagnoses (11.6%). Prostate cancer (7.1%) and colorectal cancer (6.1%) followed in frequency. Among men, lung cancer was most common, while breast cancer was the leading diagnosis in women. The study found cancer patterns vary greatly by region due to economic and lifestyle differences. This highlights the urgent need for better cancer data collection, especially in poorer countries.

[23] assessed HE4's efficacy in epithelial ovarian cancer screening using samples from 112 cancer patients and 706 controls. Compared to transvaginal ultrasound (TVU), HE4 performed better as a second-line screen, confirming 27/39 cancers with elevated CA125 levels versus 17 by TVU (P=.03). HE4 levels increased with age and smoking status, suggesting benefits from longitudinal monitoring. Combining CA125 screening with HE4 could reduce unnecessary surgeries while improving accuracy. Limitations include the relatively small sample size and potential confounding factors affecting serum HE4 concentrations in different populations. Table 1 summarizes various related works on ovarian cancer detection, focusing on the technologies, key findings, and limitations of each approach.

Table 1: Summary of Related Works

S. No	Author & Year	Title	Technology	Key Findings	Limitations
1	Feng (2024)	Design and Development of Meta-heuristic Transfer Learning techniques for Ovarian cancer detection	Integrated ML model with ResNet50 and three edge output modules	83.62% Dice similarity and ROC curve area of 0.948	Reliance on single dataset
2	Salman et al. (2024)	Deep Learning-Based Ovarian Cancer Subtype Classification Using VGG16 and MobileNetV2 with Squeeze-and-Excitation Blocks	VGG16 and MobileNetV2 with SE blocks	Enhanced performance in capturing tissue patterns with enhanced accuracy	High computational requirements
3	Xie et al. (2024)	Developing a deep learning model for predicting ovarian cancer in O-RADS US Category 4 lesions	Dual-architecture combining DeepLabV3 and YOLOv8	98.68% precision for benign masses, 96.23% for malignant masses	Performance constrained by specific dataset, limiting generalization
4	Mustafa et al. (2024)	Detection of Ovarian Cancer Using Improved Deep Learning Model	Modified VGG-16 architecture	Improved accuracy from 50% to 84% after dataset expansion	Resource-intensive
5	El-Latif et al. (2024)	A deep learning approach for ovarian cancer detection and classification relied on fuzzy deep learning	ResNet-50 with recursive feature elimination	98.99% accuracy, 99% sensitivity, 98.96% specificity	Extended training time
6	Ziyambe et al. (2023)	A DL Framework for the Prediction and Diagnosis of Ovarian Cancer in Pre- and Post-Menopausal Women	CNN-based framework	94% accuracy, 95.12% sensitivity, 93.02% specificity	Limited menopausal analysis
7	Schwartz et al. (2022)	Ovarian cancer detection using optical coherence tomography and convolutional neural networks	Three neural networks: VGG-supported feed-forward, 3D CNN, and convolutional LSTM	Best AUC of 0.81 ± 0.037 with convolutional LSTM	Moderate accuracy compared to other models
8	Jung et al. (2022)	Ovarian tumor diagnosis using deep convolutional neural networks and a denoising convolutional autoencoder	CNN with convolutional autoencoder (CNN-CAE)	97.2% accuracy, 0.9936 AUC for normal vs. tumor, 90.12% accuracy for malignant tumors	Potential scalability issue
9	Ghazal and Taleb (2022)	Feature optimization and recognition of ovarian cancer utilizing internet of medical things	Self-Organizing Map with Optimized Neural Networks	94% precision, 0.029% RMSE	Complex implementation
10	Bray et al. (2018)	Global cancer statistics 2018: GLOBOCAN estimates of incidence and mortality worldwide for 36 cancers in 185 countries.	GLOBOCAN 2018 data analysis	18.1M new cancer cases; lung cancer highest in diagnosis (11.6%) and deaths (18.4%);	Poor data quality from low-income countries
11	Urban et al. (2011)	Potential role of HE4 in multimodal screening for epithelial ovarian cancer.	HE4 serum biomarker	HE4 outperformed TVU (27/39 cancers vs. 17/39); HE4 levels affected by age and smoking	Small sample size

Building upon the strengths and limitations identified in existing research, the need for a more robust and efficient solution becomes evident. To address these gaps, the proposed methodology introduces a hybrid framework that combines Inception V3 with an improved Black Widow Optimization algorithm.

3. Proposed methodology

The suggested model comprises five primary components: (i) Data Collection Unit, (ii) Data Preprocessing, (iii) Feature Extraction using the Inception V3 framework, (iv) Hyperparameter Tuning via Black Widow Optimization, and Classification Phase for ovarian cancer subtype detection. Figure 1 depicts the entire framework of the suggested methodology.

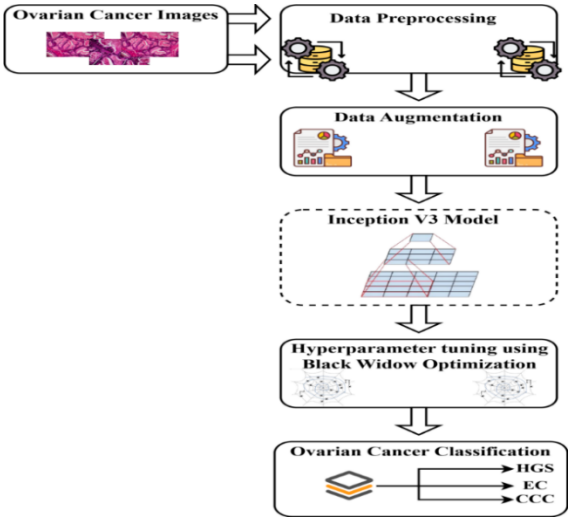


Fig. 1: Architecture for the Recommended Approach.

3.1. Materials and methods

This research utilises the UBC OCEAN dataset. The UBC Ovarian Cancer Subtype Classification and Outlier Detection (UBC-OCEAN) dataset is a specialized resource designed for advancing research in ovarian cancer classification and anomaly detection. Figure 2 shows the number of images in datasets utilized for training and testing the proposed model.

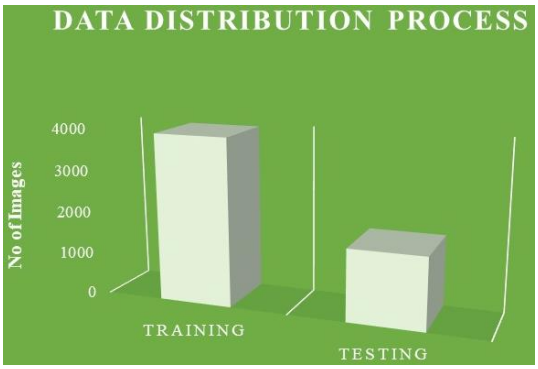


Fig. 2: Number of Ovarian Cancer Images Used for Training and Testing.

This dataset focuses on stratifying ovarian cancer into subtypes based on specific clinical and molecular features, facilitating the identification of outliers that may indicate novel or rare cancer profiles. It integrates genomic, transcriptomic, and proteomic data, providing a multidimensional view of ovarian cancer that supports comprehensive analysis. Figure 3 shows the class distribution in the dataset.

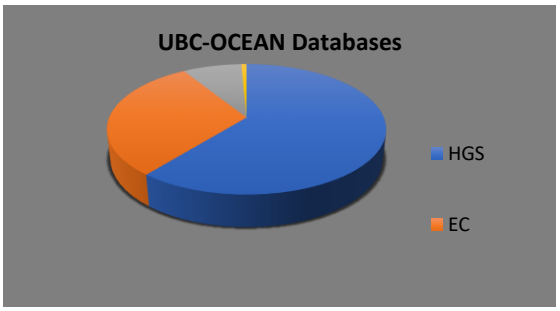
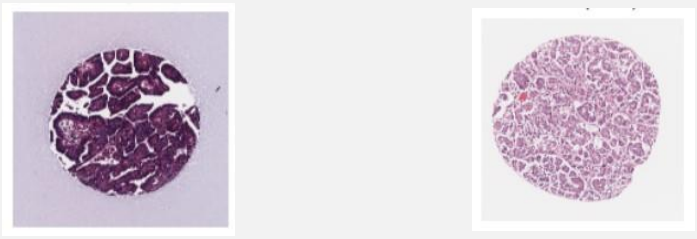
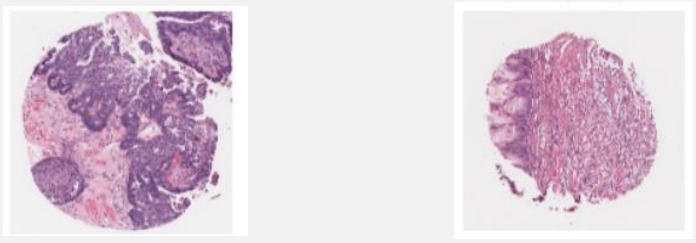
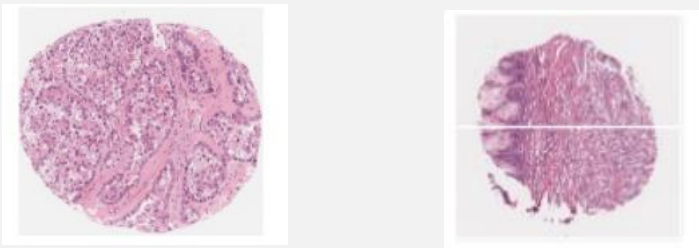


Fig. 3: Class Distribution of the Datasets.

The UBC-OCEAN dataset comprises a total of 5,634 samples, classified into three primary ovarian cancer subtypes: high-grade serous carcinoma (HGS) with 3,412 samples, endometrioid carcinoma (EC) with 1,732 samples, and clear cell carcinoma (CCC) with 490 samples. Table 2 presents sample images of ovarian cancer subtypes. The dataset also includes outlier samples that represent rare or atypical cases, enhancing its utility for anomaly detection studies. Each image in the dataset is standardized to a pixel size of 224 x 224, ensuring consistency for deep learning models and facilitating preprocessing steps such as resizing and augmentation.

Table 2: Sample Images of Ovarian Cancer Subtypes

Ovarian Cancer Subtypes	Images
High-grade serous carcinoma (HGS)	
Endometrioid carcinoma (EC)	
Clear cell carcinoma (CCC)	

3.2. Image pre-processing

Ovarian Cancer Images preprocessing techniques are employed to eliminate noise and low-quality pixels that hinder the recognition of ovarian cancer. To address this, a Pixel Intensive Testing process is utilized to remove inconsistent and noisy pixels from images. Additionally, image histogram methods are applied to enhance image quality, as they are effective across various image types. Following preprocessing, the input images undergo image augmentation in the proposed architecture. Since there is a class imbalance problem, image augmentation is performed.

3.3. Image augmentation process

Data augmentation is a highly efficient approach to mitigate this issue. During this segment, each ovarian cancer image undergoes multiple transformations, generating a substantial volume of newly enhanced training samples. affine transformations are employed to achieve efficient data augmentation. Techniques like translation, scaling, and rotation are utilized to transform the images. Since the training samples generated through augmentation often exhibit correlation, this step is crucial to addressing overfitting challenges. The below figure 4 depicts the output of both preprocess and augmentation process.

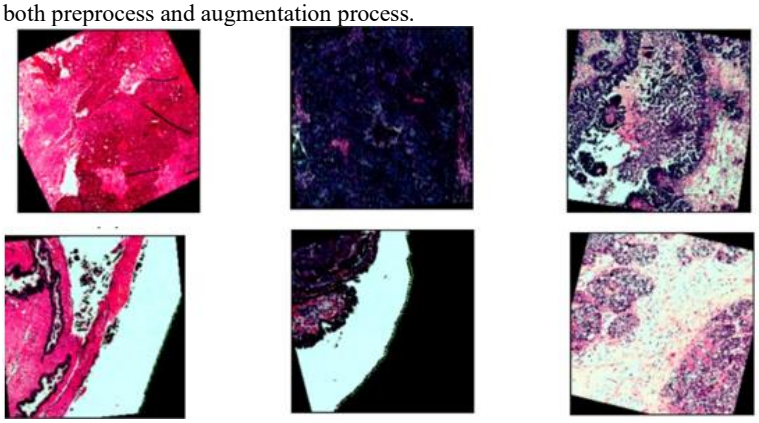


Fig. 4: Images After Pre-Processing and Augmentation.

3.4. Inception V3

Transfer Learning is an effective method in deep learning that involves taking a model trained on a large dataset and modifying or refining it to tackle a new but similar problem. This approach is particularly useful when the target dataset is small or has constrained labelled data, as it leverages the knowledge learned from the large dataset to enhance performance. The features learned by pre-trained models are general in the initial layers and become increasingly task-specific in the deeper layers. By freezing or fine-tuning these layers, the pre-trained model can be effectively adapted to the new task.

ImageNet, a large-scale visual database with millions of labelled images across thousands of categories, serves as a standard benchmark for pre-training DL models. Models pre-trained on ImageNet, such as Inception V3, have already learned a rich hierarchy of features, making them well-suited for transfer learning in diverse domains, including medical image analysis.
Inception V3 is a CNN framework that is widely utilized in transfer learning because to its ability to extract multi-scale features efficiently. Pre-trained on ImageNet, Inception V3 provides a robust feature extractor that can generalize well to medical imaging tasks. Its architecture, which includes sophisticated operations like factorized convolutions and auxiliary classifiers, enables it to process high-resolution medical images effectively while addressing challenges such as class imbalance and overfitting.
The proposed model integrates an Inception V3 block, which is specifically designed to capture local spatial features at multiple scales. Inception V3 uses various convolution kernel sizes, such as 1x1, 3x3, and 5x5, along with pooling operations to learn multi-scale representations from the input image. Each convolution block in the Inception V3 architecture as depicted in Figure 5, is followed by batch normalization, PReLU activation, and global pooling layers. These blocks enable the model to extract rich features and reduce the computational complexity by applying dimensionality reduction via 1x1 convolutions before larger convolutions. The convolution process involves a kernel sliding over the input image, performing elementwise multiplication and summing the results to generate a single output pixel. In Inception V3, multiple kernels of different sizes (1x1, 3x3, and 5x5) are applied in parallel, and their outputs are concatenated along the depth angles. This multi-path approach permits the network to capture attributes at different scales and resolutions, which elevates its capability to recognize complex patterns in medical images.

The convolution operation is generally represented as:

$$y(i,j) = \sum_m \sum_n x(i+m, j+n) \cdot w(m,n) \quad (1)$$

Where x(i,j) is the input image, w(m,n) is the kernel or filter, y(i,j) is the output after convolution at lovation (i,j) m and n are the kernel's angles.

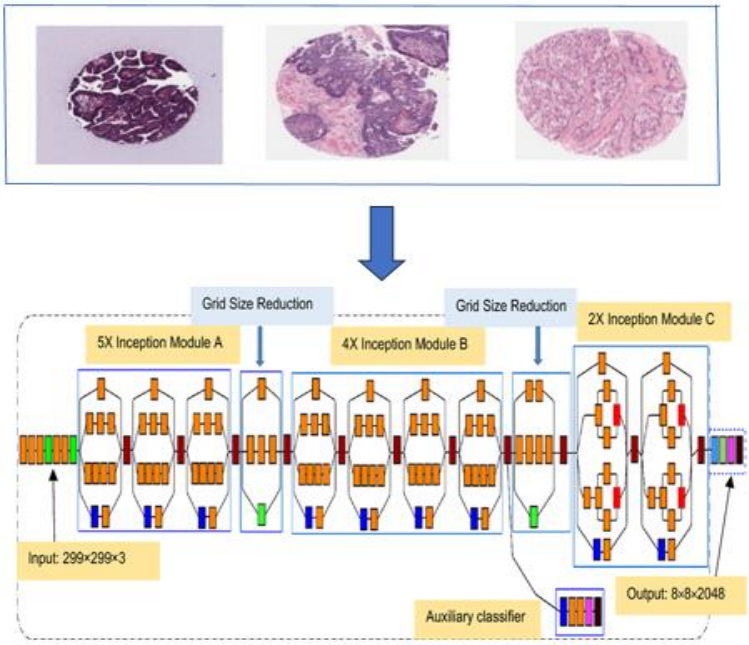


Fig. 5: Architecture Diagram of Inception V3.

Table 3: Convolutional Parameters Used for Constructing Inception V3 Layers

Layers	Kernel Size	Output Images
Conv2D (Inception Module 1)	1x1	299x299x32
Conv2D (Inception Module 2)	3x3	149x149x64
Conv2D (Inception Module 3)	5x5	73x73x128
Global Average Pooling Layers 2D	2x2	73x73x128
Conv2D (Inception Module 4)	1x1	35x35x256
Global Average Pooling Layers 2D	2x2	35x35x256
Conv2D (Inception Module 5)	3x3	17x17x512
Global Average Pooling Layers 2D	2x2	17x17x512

Table 3 outlines the Convolutional Parameters Used for Constructing Inception V3 Layers. The Inception V3 model, through its multi-path structure, efficiently captures spatial features at various levels, pursued by a Global Average Pooling (GAP) layer to minimise the dimensionality of the feature maps. This helps overcome overfitting and minimizes the computational complexity of subsequent layers. The resulting feature vectors are passed through fully connected layers for classification, yielding improved accuracy and robustness in Ovarian cancer image.

3.4.1. Factorization into smaller convolutions

In Inception V3, factorization into smaller convolutions refers to breaking down larger convolutional operations into smaller, more efficient ones. A 5x5 convolution can be factorized into two 3x3 convolutions, which reduces the computational cost and improves efficiency without compromising the quality of the feature extraction. The intuition behind this factorization is to capture similar feature patterns while reducing the number of computations required.

In Ovarian cancer image, factorizing larger convolutions into smaller ones aids the model recognize sophisticated structures and details in the Ovarian images with reduced computational complexity. This results in faster processing, which is crucial for handling high-resolution medical images, and also helps the model achieve better performance by reducing overfitting. Here spatial factorisation is deployed to enhance further performance and the auxiliary classifier has been added. Table 4 illustrates the factorization of larger convolutions into smaller ones, such as breaking down 5x5 and 7x7 convolutions into combinations of 3x3 convolutions.

Table 4: Factorization into Smaller Convolutions

Original Convolution	Factorized Convolutions
5x5 Conv	3x3 Conv + 3x3 Conv
7x7 Conv	3x3 Conv + 3x3 Conv + 3x3 Conv

3.4.2. Efficient grid size reduction

Efficient grid size reduction refers to using pooling and stride-based convolutions to minimise the spatial resolution of the feature maps, allowing the model to focus on high-level features and making the computation more efficient. Reducing the grid size helps to compress the information and decrease the number of computations, which is particularly useful for handling large images with high resolution. By efficiently reducing the grid size, the proposed model can make predictions faster without sacrificing accuracy in detecting important medical patterns.

3.5. Black widow optimization

Black Widow Optimization (BWO) is a nature-inspired metaheuristic algorithm based on the mating and cannibalistic behaviour of black widow spiders. It operates by generating an initial population, mimicking mating to create offspring, and then applying cannibalism to eliminate weaker individuals, ensuring survival of the fittest. Figure 6 illustrates the working mechanism of BWO algorithm.

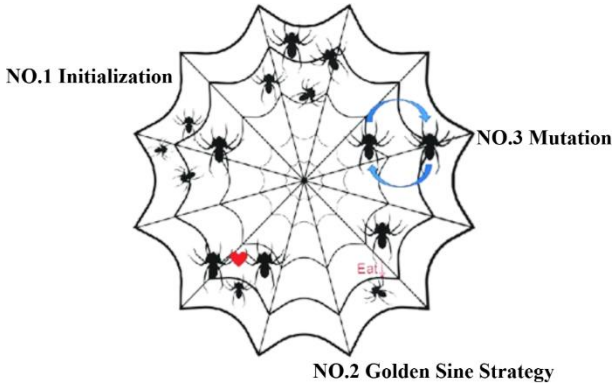


Fig. 6: Workflow of Black Widow Optimization.

3.5.1. Improved black widow optimization algorithm

To address the limitations of the standard BWOA, including inadequate robustness and sluggish convergence rates, an enhanced version of BWOA has been introduced. This improved approach integrates a double chaotic map, a golden sine exploration mechanism, and a Cauchy barycenter reverse differential mutation operator. These modifications efficiently mitigate the premature convergence issue observed in the conventional BWOA, thereby enhancing the algorithm's overall optimization capabilities.

3.5.1.1. Population initialization through double chaotic map

The initial diversity of a inhabitants plays a crucial role in widening the algorithm's search space, enhancing optimization performance, and accelerating convergence speed. In the traditional BWOA, the random initialization of inhabitants positions often results in an uneven distribution of black widows, which negatively impacts the algorithm's exploitation capabilities. Chaotic motion mapping, characterized by its randomness, regularity, and ergodicity, allows a non-repetitive traversal of a given range, effectively addressing the limitations of random initialization method. Currently, many researchers leverage conventional chaotic map models, such as logistic maps and sine maps, for initializing optimization algorithm populations. This approach mitigates the drawbacks of random initialization while improving the convergence rate of the algorithm. The value distribution for logistic and sine maps over the interval [0, 1] is non-uniform. Such uneven traversal reduces optimization efficiency and hampers the identification of optimal solutions, particularly when the global optimum is located away from the boundaries of the search range. To overcome this, a novel dual-chaotic map strategy as described in Eq. (2). Figure 7 demonstrates that the particles generated using this strategy exhibit superior diversity and a more uniform distribution across the search space, thereby significantly improving the algorithm's optimization efficiency.

$$\begin{cases} o_{k+1} = u \cdot o_k(1 - o_k) \\ y_{k+1} = \frac{\omega}{4}\sin(\pi \cdot y_k) \\ z_{k+1} = \mathrm{mod}(o_{k+1} + y_{k+1}, 1) \end{cases} \quad (2)$$

The variables x_k, y_k and z_k collectively represent the k-th number of chaotic, where $\omega \in (0,4]$ and u = 4. The function mod () refers to the residue operation. It is important to note that values such as 0, 0.25, 0.5, 0.75, and 1 act as boundary points within the definition domain and are excluded from the mapping process.

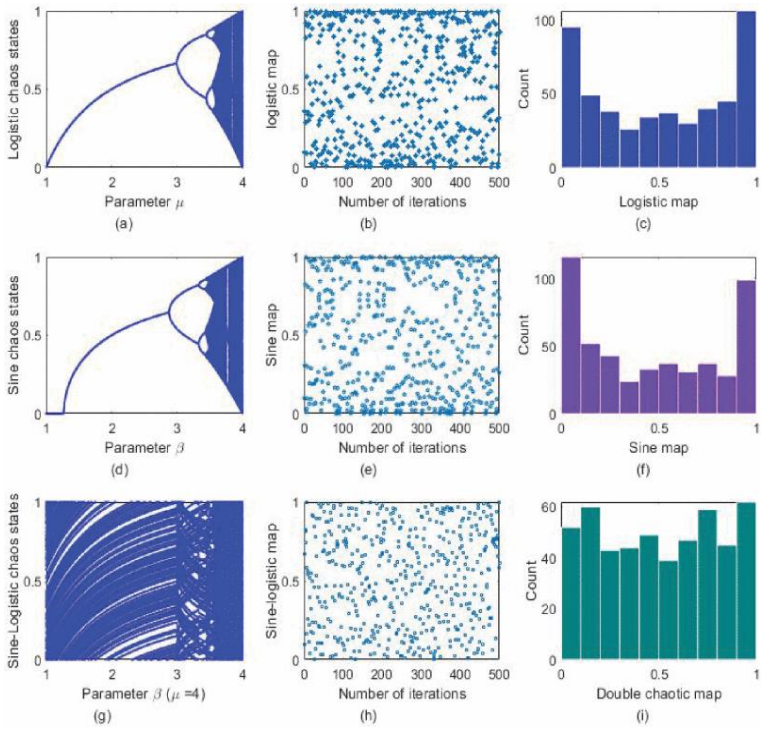


Fig. 7: Sequence Distribution and Bifurcation Analysis of the Chaotic System.

The initial placement of a BW entity is represented by z_{k+1}, determined a linear transformation as depicted in Equation (3).

$$\vec{o}_i = lb_i + (ub_i - lb_i) \times z_{k+1} \tag{3}$$

where ubi and lbi represent the upper and lower limits of the search space.

3.5.1.2. The golden sine guidance strategy

To fully utilize the differential information among optimal location and the spider, the golden sine approach is incorporated. This approach ensures a gradual progression toward the optimal solution, mitigating premature convergence inherent in the original algorithm, thereby enhancing its optimization efficiency. Spiders' movement on their web is categorized into linear and spiral motions. Upon receiving cues from a potential mate, a black spider adopts spiral motion to reach the optimal location $\vec{o}_*(t)$, which serves as the guiding coordinate during this motion.

Although this strategy can expedite the convergence speed in the later phases of optimization, it often leads to a rapid clustering of spider individuals within the search space. This phenomenon reduces population diversity and significantly increases the likelihood of becoming trapped in local optima. To address this limitation, the golden sine approach is recommended to refine the movement roadmap of spiders. Unlike other metaheuristic procedures, Golden-SA leverages the golden section coefficient during position updates, thereby enabling a deeper search space exploration and enhancing optimization precision.

The golden sine search is formulated as given in the equation (4)

$$\begin{cases} o_i^{t+1} = o_i^t \times |\sin(J_1)| + J_2 \times \sin(J_1) \times |\lambda_1 \times P_*^t - \lambda_2 \times o_i^t| \\ \lambda_1 = a + (1-\tau) \times b \\ \lambda_2 = (1-\tau) \times a + \tau \times b \\ \tau = \sqrt{5} - 1/2 \end{cases} \tag{4}$$

In the given equation, P_*^t represents the historically optimal position, while x_i^t depicts the location of the i-th entity during the t-th loop. R_1 & R_2 are stochastic variables, where $J_1 \in [0,2\pi]$ signifies the magnitude of the i-th entity's movement, and $J_2 \in [0,\pi]$ defines the route for updating the entity's location. The parameter τ is known as the golden ratio. In the Gold-SA algorithm, the initial values of a and b are conventionally set to $-\pi$ and π, Correspondingly. Two coefficients, $\lambda 1$and $\lambda 2$, are derived after incorporating the golden ratio. These coefficients are dynamically adjusted based on changes in the objective function value. This adjustment mechanism helps refine the search region and enables the current value to converge closer to the desired target. By integrating the golden sine search approach, the updated location equation for the BW spider's motion across the web is formulated as,

$$\vec{o}_i(t+1) = \begin{cases} \vec{o}_*(t) - m\vec{o}_{r_1}(t) \text{ if rand} \le 0.3 \\ \vec{o}_i(t) \times |\sin(J_1)| + J_2 \times \sin(J_1) \times \cdots \\ |\lambda_1 \times \vec{o}_*(t) - \lambda_2 \times \vec{o}_i(t)| \text{ in other cases} \end{cases} \tag{5}$$

As indicated in Equation (5), when the i-th spider shifts towards the position of its potential mate on the web, it exchanges data with the most optimal entity each time its location is upgraded. Every spider is capable of fully understanding the distinction among best entity and the itself.

Moreover, the movement's distance and direction can be regulated by adjusting parameters J1, J2, λ1, and λ2. This adjustment enables the gradual narrowing of the search space. Such control can notably enhance the speed of convergence and the overall efficiency of the optimization process.

3.5.1.3. Cauchy barycenter reverse (CBR) differential mutation operator

The inhabitant's variety in the BWOA tends to decline significantly as the iteration progresses. To address this issue, expand the search space, and prevent the approach from getting trapped in local optima, this study proposes the incorporation of the CBR differential mutation strategy to produce mutated spiders. The centroid is defined as follows: Consider the values of N spiders in the j-th angle, denoted as (o1j, o2j, …, oNj), where N is the inhabitants size and D represents the number of angles. The j-th angles is given by Eq. (6). Thus, the centroid of the inhabitants is represented as Zg = (Z1, Z2, …, Zj, …, ZD).

$$Z_j = \frac{o_{1j}+o_{2j}+\cdots+o_{Nj}}{N} \tag{6}$$

The location of the i-th spider is represented as $o_i=(o_{i1},o_{i2},\ldots,o_{ij},\ldots,o_{iD})$where the reverse computation of the center of gravity can be arranged as folows:

$$o_{oj} = 2 * \text{cauchy}(0,1) * Z_j - x_{ij} \tag{7}$$

In Eq. (6), to prohibit the reverse solution from generating any varied entities, which could negatively impact the convergence speed of the approach, a dynamic coefficient based on the standard Cauchy distribution is represented. The inclusion efficiently reduces the likelihood of location recurrence, broadens the search space, and enhances the approach's global exploration capability. The iterative processes involving mutation, crossover, and selection. The population mutation is determined by the weighted sum of the difference among any two randomly selected entity vectors in the search space, as well as the third selected at random entity vector. The entity in its transformed state is arranged as,

$$o_{new_i} = o_{r1} + F \cdot (o_{r2} - o_{r3}) \tag{8}$$

The scaling factor is represented by F. The specific index is an integer value from the set new_i $\neq r_1 \neq r_2 \neq r_3 \in$ [1, PopSize], where x_{r1} denotes the base vector and the variance vector is given by $x_{r2} - x_{r3}$.
The Cauchy reverse mutation applied to the center of gravity helps preserve the diversity of the Inhabitants. During the early stages of the loop, the variance among entities in the Inhabitants are significant, allowing the mutated spider to broaden the search space. In later iterations, the introduction of mutated spiders helps ascertain population diversity. Furthermore, while the differential evolution approach relies on the variations among two randomly chosen entities as the varied vector, it overlooks the route of this vector. As a result, the differential mutation operator enhances the algorithm's search capability to some extent, it can lead to the algorithm becoming trapped in a local optimum as the iterations progress.
A novel mutation operator, known as the CBR differential mutation operator, is introduced by integrating the strengths of the two previously mentioned mutation strategies. This operator generates a mutated solution near the center of gravity of the current Inhabitants. The operator is represented in Equation (9):

$$O_{new} = Z_g + F^*(O_{m_2} - O_{worst}) + F^*(O_{best} - O_{m_1}) \tag{9}$$

The center of gravity of the Inhabitants is denoted as Zg, and F represents the scaling factor, which is randomly opted within the interval [0, 2]. Two individuals are chosen randomly along with their reversed count erparts, and these are ranked relies on their fitness values from the best to the worst: Obest, Om1, Om2, and Oworst. Equation (9) portrays that its expression is influenced by the fitness values of the four opted entities, beginning from the inhabitant's center of gravity and advancing towards the optimal entity, Obest. The concept of CBR learning promotes a reverse solution that is farther from local extreme points, enhancing population diversity and thus improving the algorithm's search capability, preventing it from falling into local optima. The difference vector set moves towards Obest. Consequently, the new mutation operator, known as the Cauchy barycenter reverse differential mutation strategy. When these hybrid strategies are applied to solve engineering-constrained optimization problems, the Improved BWOA demonstrates effectively balancing global exploration with local exploitation.

3.6. Hyper parameter tuned learning process

Hyperparameter tuning is essential for identifying the optimal parameters for the model, reducing its complexity, and improving its performance. This process is carried out before the model's training phase. In this research, the hyperparameters being fine-tuned comprise the number of hidden units, dropout rate, batch size, epochs and the number of hidden layers. Metaheuristic optimization techniques are utilized to refine these network parameters to enhance the efficacy of ovarian cancer detection. The weights of the neural networks used for classification are optimized by utilizing Black widow optimization algorithms. At first, the training network selects hyperparameters at random. The fitness of the recommended approach is evaluated using a fitness function. The tuning parameters are determined through an iterative process, and the iteration wrapped up when the fitness function meets the convergence criteria outlined in equation (10).

$$\text{Fitness Function} < \text{RMSE}(\text{Prdeicted value} - \text{Actual Value}) \tag{10}$$

4. Implementation details

The proposed network model in this research was developed using Keras with TensorFlow as the backend. Table 5 presents the hyperparameters utilized for training the approach.

Table 5: Hyper Parameters Used for Training the Proposed Model

Hyperparameters used	Specifications
Initial learning rate	0.001
Epochs count	300
Batch Size	32
Optimizer	IBWO
Momentum	0.002

At the training stage, the early stopping technique was employed to halt training prematurely and mitigate the risk of overfitting. Varied augmented images were utilized to elevate the training process. The entire approach was implemented on a PC workstation equipped with 16GB RAM, a 2TB SSD, an Intel i7 processor, an NVIDIA GeForce RTX GPU, and an operating frequency of 3.4 GHz.

4.2. Evaluation metrics

The performance of the recommended approach is examined by utilizing key metrics like precision, recall, accuracy, F1-score and specificity. These results are directly compared with other advanced ensemble feature selection techniques to emphasize the approach's advantages. Furthermore, all relevant performance metrics and associated costs are analysed to demonstrate the approach's superior effectiveness and minimal resource requirements. Table 6 provides the computational formulas used to calculate these performance metrics.

Table 6: Performance Measures Utilized in the Evaluation

Performance Measures	Expression
$A_{ccuracy}$	$\frac{T_P+T_N}{T_P+T_N+F_P+F_N}$
R_{ecall}	$\frac{T_P}{T_P+F_P}$ x100
$S_{pecificity}$	$\frac{T_N}{T_N+F_P}$
$P_{recision}$	$\frac{T_N}{T_P+F_P}$
$F_{1\text{-}Score}$	$2.\frac{P_{recison}*R_{ecall}}{P_{recision}+R_{ecall}}$

TP & TN are True Positive & negative, FP & FN are False Positive& negative.

Prediction can be divided into four components: T_P, where the values are truly recognized as positive and are genuinely positive; F_P, where the values are mistakenly classified as positive when they are actually negative; F_N, where true positive values are incorrectly predicted as negative; and T_N, where the predicted negative values are accurately recognized as negative in reality.

4.3. Experimental outcomes

Figure 8 portrays the validation performance of the proposed algorithm under two different data splits: a) 80% training & 20% Testing Data b) 70% training & 30% Training Data. The results highlight the algorithm's effectiveness in maintaining robust performance across varying data partitions.

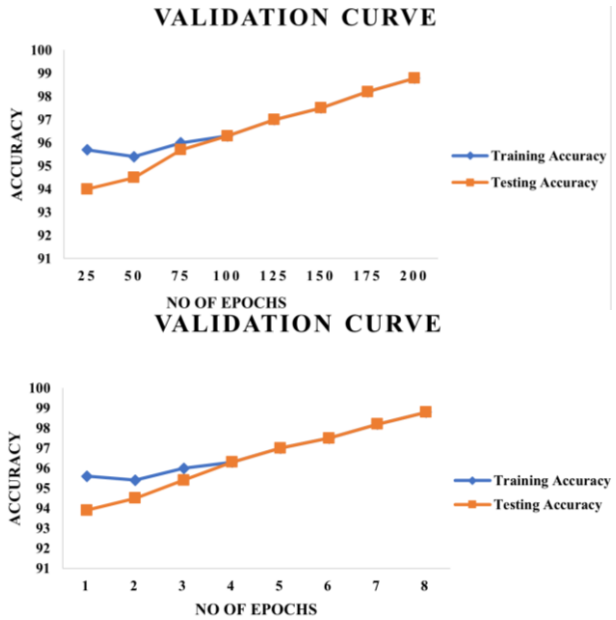


Fig. 8: Validation Performance of the Proposed Algorithm A) 80% Training & 20% Testing Data B) 70% Training & 30% Training Data.

The suggested model's effectiveness is assessed against existing DL models, including VGG16 [24], ResNet34[25], MobileNet [26], GoogleNet [27] and DenseNet [28], to establish the algorithm's superiority. Figure 9 illustrates the comparison of computational complexity in terms of training time between different models over varying epochs. The proposed model consistently demonstrates lower training time compared to existing architectures like VGG16, ResNet34, and DenseNet. This highlights the efficiency of the proposed model in reducing computational overhead, making it suitable for real-time and resource-constrained applications. Figure 10 provides a statistical comparison of different approaches. It demonstrates the proposed algorithm's notable consistency and robustness across varied scenarios.

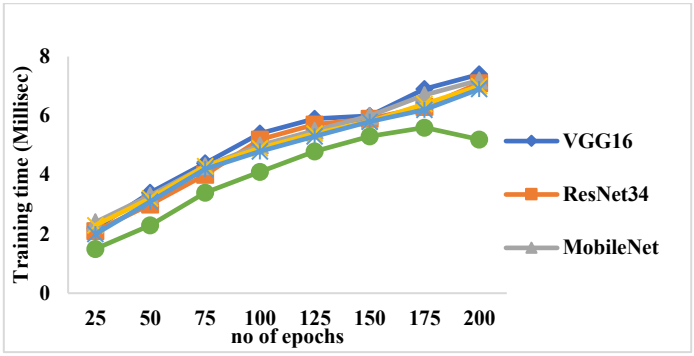


Fig. 9: Comparison of Computational Complexity

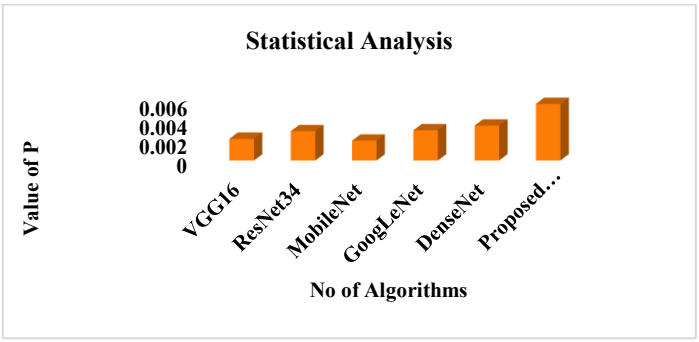


Fig. 10: Statistical Analysis of the Varied Optimization Approaches

Table 7: Average Performance Metrics of the State-of-the-Art Methods

Algorithms	Performance Metrics				
	Accuracy	Precision	Recall	Specificity	F1-score
VGG16	0.81	0.78	0.80	0.75	0.73
ResNet34	0.82	0.80	0.84	0.83	0.81
MobileNet	0.80	0.82	0.83	0.82	0.85
GoogLeNet	0.81	0.80	0.84	0.83	0.84
DenseNet	0.91	0.89	0.87	0.88	0.865
Proposed Model	0.9879	0.9878	0.9879	0.9879	0.9878

Table 7 presents the average performance metrics of state-of-the-art methods in classifying cancer images. These metrics comprise a comparative analysis of the approach's efficacy in accurately identifying cancerous and non-cancerous images, highlighting their strengths and limitations in terms of F1-score, recall, precision and overall accuracy. Figure 11 depicts the confusion matrix of the recommended approach in detecting ovarian cancer.

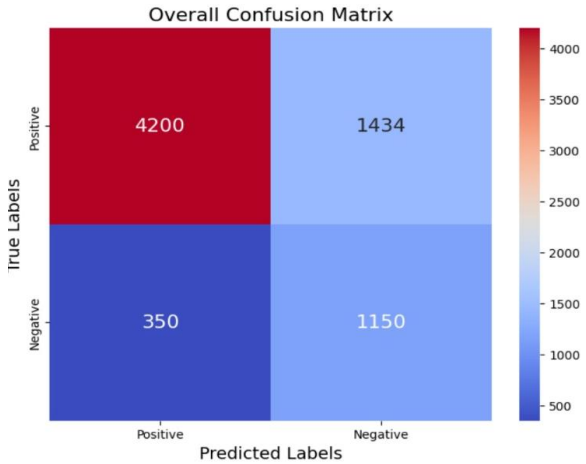


Fig. 11: Confusion Matrix of the Recommended Approach in Identifying the Cancer Entities.

Table 8: Performance Metrics of the State-of-the-Art Methods (Malignant)

Algorithms	Performance Metrics				
	Accuracy	Precision	Recall	Specificity	F1-score
VGG16	0.812	0.784	0.81	0.761	0.74
ResNet34	0.83	0.802	0.842	0.831	0.82
MobileNet	0.81	0.83	0.832	0.821	0.851
GoogLeNet	0.81	0.801	0.84	0.833	0.84
DenseNet	0.92	0.90	0.88	0.885	0.868
Proposed Model	0.9879	0.9878	0.9879	0.9879	0.9878

Table 9: Average Performance Metrics of the Cutting-Edge Approaches (Benign)

Algorithms	Performance Metrics				
	$A_{ccuracy}$	$P_{recision}$	R_{ecall}	$S_{pecificity}$	$F_{1\text{-}score}$
VGG16	0.811	0.79	0.804	0.76	0.731
ResNet34	0.821	0.81	0.841	0.84	0.812
MobileNet	0.804	0.825	0.84	0.821	0.851
GoogLeNet	0.82	0.80	0.841	0.834	0.85
DenseNet	0.911	0.893	0.87	0.89	0.867
Proposed Model	0.9879	0.9878	0.9879	0.9879	0.9878

Table 8 summarizes the average performance metrics of cutting-edge approaches in classifying malignant cases, reflecting their ability to accurately detect and distinguish malignant cancer images. Similarly, Table 9 presents the average performance metrics for classifying benign cases, showcasing the methods' effectiveness in identifying non-cancerous images. The optimized feed-forward networks, combined with the proposed segmentation model, have demonstrated improved performance compared to other models. Together, these tables provide a comprehensive comparison of the methods' capabilities in addressing both malignant and benign cases.

4.4. Statistical outcomes

Table 10 portrays a comparative analysis of the performance of various algorithms based on key indicators, including their best, worst, mean, median, standard deviation, and variance values. It highlights the proposed model's enhanced performance, demonstrating better convergence, consistency, and robustness compared to other algorithms.

Table 10: Indicator Performance of Different Algorithms

Algorithm	Best	Worst	Mean	Median	SD	Variance
VGG16	0.7491	0.6483	0.73010	0.024912	0.068271	5.3×10^{-6}
ResNet34	0.72220	0.64490	0.69234	0.019324	0.075433	6.5×10^{-6}
MobileNet	0.75720	0.62580	0.65572	0.034950	0.065561	4.26×10^{-5}
GoogLeNet	0.78965	0.67990	0.71549	0.029343	0.0534502	3.136×10^{-4}
DenseNet	0.84590	0.71512	0.72502	0.033593	0.043542	2.923×10^{-4}
Proposed Model	0.9879	0.81302	0.85740	0.068513	0.0398503	1.28950×10^{-4}

5. Conclusion

In this research article, a hybrid framework integrating Inception V3 for transfer learning with the Black Widow Optimization algorithm was introduced for the effective classification of ovarian cancer subtypes. This integration aims to enhance classification accuracy by leveraging the deep feature extraction capabilities of Inception V3 and the optimization strengths of Black Widow Optimization for refining model parameters. The model was trained on the UBC-OCEAN dataset, comprising 5,634 samples across three primary ovarian cancer subtypes and outlier cases. Various performance metrics, including precision, recall, F1-score and accuracy were examined, with the recommended approach achieving a classification accuracy of 98.7%, precision of 98.7%, recall of 98.7%, and F1-score of 98.7%. Experimentation outcomes demonstrated the supremacy of the recommended approach examined to conventional methods. However, the model's generalizability may be limited due to potential dataset bias, highlighting the need for validation across larger and more diverse datasets. Future enhancements could involve incorporating multi-modal data sources to strengthen overall diagnostic reliability. The model's computational efficiency supports its potential for integration into clinical workflows. Although real-world deployment remains a future objective, the modular design ensures compatibility with existing systems. Additionally, incorporating explainable AI techniques will enhance clinical trust by providing interpretable and transparent predictions.

References

[1] Zhang, L., Wang, S., & Liu, X. (2023). "Transfer Learning with Inception v3 for Ovarian Cancer Classification Enhanced by Meta-Heuristic Optimization." Journal of Medical Imaging and Health Informatics, 13(2), 345-352.

[2] Chen, H., Zhao, Y., & Li, J. (2023). "Meta-Heuristic Optimized Transfer Learning Framework for Early Detection of Ovarian Cancer." IEEE Access, 11, 56789-56798.

[3] Kumar, R., Gupta, S., & Verma, P. (2022). "Ovarian Cancer Detection Using Inception v3 and Enhanced Optimization Techniques." International Journal of Computational Intelligence Systems, 15(4), 789-798.

[4] Singh, A., & Kaur, P. (2023). "Hybrid Meta-Heuristic and Transfer Learning Approach for Ovarian Tumor Classification." Expert Systems with Applications, 207, 117921. https://doi.org/10.1016/j.eswa.2022.117921.

[5] Patel, M., & Shah, S. (2022). "Optimized Transfer Learning Model for Ovarian Cancer Diagnosis Using Inception v3." Computers in Biology and Medicine, 145, 105409. https://doi.org/10.1016/j.compbiomed.2022.105409.

[6] Li, X., Yang, F., & Zhou, Q. (2023). "Black Widow Optimization-Based Transfer Learning for Ovarian Cancer Image Classification." Pattern Recognition Letters, 162, 45-52. https://doi.org/10.1016/j.patrec.2023.01.005.

[7] Ahmed, S., & Khan, M. (2022). "Meta-Heuristic Driven Inception v3 Model for Accurate Ovarian Cancer Detection." Biomedical Signal Processing and Control, 75, 103591. https://doi.org/10.1016/j.bspc.2022.103591.

[8] Wang, Y., & Luo, Z. (2023). "Enhanced Transfer Learning Approach Using Inception v3 and Black Widow Optimization for Ovarian Cancer Classification." IEEE Transactions on Biomedical Engineering, 70(3), 789-798.

[9] Zhao, L., & Huang, J. (2022). "Application of Meta-Heuristic Algorithms in Transfer Learning for Ovarian Cancer Detection." Artificial Intelligence in Medicine, 128, 102312. https://doi.org/10.1016/j.artmed.2022.102312.

[10] Gupta, D., & Mehta, P. (2023). "Ovarian Cancer Detection Using Inception v3 and Black Widow Optimization: A Transfer Learning Approach." Journal of Healthcare Engineering, 2023, Article ID 1234567.

[11] Liu, H., & Zhang, Y. (2022). "Integrating Meta-Heuristic Optimization with Transfer Learning for Improved Ovarian Cancer Diagnosis." Computers in Biology and Medicine, 140, 105114. https://doi.org/10.1016/j.compbiomed.2021.105114.

[12] Roy, S., & Banerjee, S. (2023). "A Novel Transfer Learning Framework Using Inception v3 and Black Widow Optimization for Ovarian Cancer Detection." IEEE Journal of Biomedical and Health Informatics, 27(1), 123-132.

[13] Feng, Y. An integrated machine learning-based model for joint diagnosis of ovarian cancer with multiple test indicators. J Ovarian Res 17, 45 (2024). https://doi.org/10.1186/s13048-024-01365-9.

[14] Salman Mohammad Abdullah, Abdullah Al Masum, Nayem Uddin Prince, Labonno Akter Mim (2024). "Deep Learning-Based Ovarian Cancer Subtype Classification Using VGG16 and MobileNetV2 with Squeeze-and-Excitation Blocks", Journal of Angiotherapy, 8(8),1-11, 9898https://doi.org/10.25163/angiotherapy.889898.
[15] Xie, W., Lin, W., Li, P. et al. Developing a deep learning model for predicting ovarian cancer in Ovarian-Adnexal Reporting and Data System Ultrasound (O-RADS US) Category 4 lesions: A multicenter study. J Cancer Res Clin Oncol 150, 346 (2024). https://doi.org/10.1007/s00432-024-05872-6.
[16] Mustafa, M.A., Allami, Z.F., Arabi, M.Y., Abdulhasan, M.M., Ghadir, G.K., Al-Tmimi, H.M. (2024). Detection of Ovarian Cancer Using Improved Deep Learning Model. In: Botto-Tobar, M., Zambrano Vizuete, M., Montes León, S., Torres-Carrión, P., Durakovic, B. (eds) International Conference on Applied Technologies. ICAT 2023. Communications in Computer and Information Science, vol 2049. Springer, Cham. https://doi.org/10.1007/978-3-031-58956-0_6.
[17] El-Latif, E.I.A., El-dosuky, M., Darwish, A. et al. A deep learning approach for ovarian cancer detection and classification based on fuzzy deep learning. Sci Rep 14, 26463 (2024). https://doi.org/10.1038/s41598-024-75830-2.
[18] Ziyambe, B., Yahya, A., Mushiri, T., Tariq, M. U., Abbas, Q., Babar, M., Albathan, M., Asim, M., Hussain, A., & Jabbar, S. (2023). A Deep Learning Framework for the Prediction and Diagnosis of Ovarian Cancer in Pre- and Post-Menopausal Women. Diagnostics (Basel, Switzerland), 13(10), 1703. https://doi.org/10.3390/diagnostics13101703.
[19] Schwartz, D., Sawyer, T.W., Thurston, N. et al. Ovarian cancer detection using optical coherence tomography and convolutional neural networks. Neural Comput & Applic 34, 8977–8987 (2022). https://doi.org/10.1007/s00521-022-06920-3.
[20] Jung, Y., Kim, T., Han, MR. et al. Ovarian tumor diagnosis using deep convolutional neural networks and a denoising convolutional autoencoder. Sci Rep 12, 17024 (2022). https://doi.org/10.1038/s41598-022-20653-2.
[21] Ghazal, T. M., & Taleb, N. (2022). Feature optimization and identification of ovarian cancer using internet of medical things. Expert Systems, 39(9), e12987. https://doi.org/10.1111/exsy.12987.
[22] Bray, F., Ferlay, J., Soerjomataram, I., Siegel, R. L., Torre, L. A., & Jemal, A. (2018). Global cancer statistics 2018: GLOBOCAN estimates of incidence and mortality worldwide for 36 cancers in 185 countries. CA: a cancer journal for clinicians, 68(6), 394–424. https://doi.org/10.3322/caac.21492.
[23] Urban, N., Thorpe, J. D., Bergan, L. A., Forrest, R. M., Kampani, A. V., Scholler, N., O'Briant, K. C., Anderson, G. L., Cramer, D. W., Berg, C. D., McIntosh, M. W., Hartge, P., & Drescher, C. W. (2011). Potential role of HE4 in multimodal screening for epithelial ovarian cancer. Journal of the National Cancer Institute, 103(21), 1630–1634. https://doi.org/10.1093/jnci/djr359.
[24] Abdullah, S. M., Al Masum, A., Prince, N. U., & Mim, L. A. (n.d.). Deep learning-based ovarian cancer subtype classification using VGG16 and MobileNetV2 with squeeze-and-excitation blocks. Angiotherapy. https://doi.org/10.25163/angiotherapy.889898.
[25] Miao, Kuo & Zhao, Ning & Lv, Qian & He, Xin & Xu, Mingda & Dong, Xiaoqiu & Li, Dandan & Shao, Xiaohui. (2023). Prediction of benign and malignant ovarian tumors using Resnet34 on ultrasound images. Journal of Obstetrics and Gynaecology Research. 49. 10.1111/jog.15788. https://doi.org/10.1111/jog.15788.
[26] Almujally, Nouf & Alzahrani, Abdulrahman & Hakeem, Abeer & Attiah, Afraa & Umer, Muhammad & Alsubai, Shtwai & Polsinelli, Matteo & Ashraf, Imran. (2024). Selective feature-based ovarian cancer prediction using MobileNet and explainable AI to manage women healthcare. Multimedia Tools and Applications. 1-22. 10.1007/s11042-024-19286-6. https://doi.org/10.1007/s11042-024-19286-6.
[27] Hira, M. T., Razzaque, M. A., & Sarker, M. (2024). Ovarian cancer data analysis using deep learning: A systematic review. Engineering Applications of Artificial Intelligence, 138(Part A), 109250. https://doi.org/10.1016/j.engappai.2024.109250
[28] He, X., Bai, XH., Chen, H. et al. Machine learning models in evaluating the malignancy risk of ovarian tumors: a comparative study. J Ovarian Res 17, 219 (2024). https://doi.org/10.1186/s13048-024-01544-8.